Korean J. Chem. Eng., 38(1), 163-169 (2021)
DOI: 10.1007/s11814-020-0687-y

pISSN: 0256-1115
eISSN: 1975-7220

Synthesis and photocatalytic performance of Bi_2WO_6/BiOX (X=Cl, Br, I) composites for RhB degradation under visible light

Leila Derikvand and Nemat Tahmasebi†

Department of Physics, Jundi-Shapur University of Technology, Dezful, Iran
(*Received 21 May 2020 • Revised 31 August 2020 • Accepted 3 October 2020*)

Abstract−The present study examined the effects of adding bismuth oxyhalides, BiOCl, BiOBr and BiOI, on the photocatalytic properties of Bi_2WO_6. The samples were synthesized using a simple one-stage hydrothermal method. The samples were characterized using X-ray diffraction (XRD), scanning electron microscopy (SEM), diffused reflectance spectroscopy (DRS) and the nitrogen absorption/desorption technique. The activity of the products on the photocatalytic degradation of an aqueous Rhodamine B (RhB) solution was then investigated under visible light irradiation. The results showed the higher photocatalytic efficiency of the hybrid Bi_2WO_6/BiOBr sample compared to that of other compounds, as approximately 97% of RhB molecules were degraded after 80 minutes of irradiation in the presence of this sample. Under the same conditions, pure Bi_2WO_6 and hybrid samples of Bi_2WO_6/BiOCl and Bi_2WO_6/BiOI, respectively, degraded 40%, 60% and 20% of dye molecules in the solution. The better performance of this sample compared to that of the others can be explained by its larger effective surface area and the strong interaction between Bi_2WO_6 and BiOBr. Furthermore, a test conducted to determine active species in photocatalytic reactions showed that superoxide radicals played the main role in the degradation of RhB molecules by hybrid Bi_2WO_6/BiOBr photocatalyst.

Keywords: Hydrothermal, Bi_2WO_6, Bismuth Oxyhalide, Photocatalyst

INTRODUCTION

In the past decade, the potential of semiconductor photocatalysts for energy storage and degrading environmental pollutants has attracted the attention of researchers [1-3]. The unique physicochemical properties of titanium oxide (TiO_2) have caused this semiconductor to be extensively used for producing photocatalysts. The limitations of this semiconductor include (1) its relatively high rate of electron-hole recombination which 90% of photogenerated electron-hole pairs may rapidly recombine within 10 ns [4,5], and (2) its optical gap being as large as 3.2 eV, which degrades its photocatalytic performance under visible light irradiation that comprises 43% of solar radiation [6,7]. To date, different strategies such as metal or non-metal doping and the combination of TiO_2 with other semiconductors to form heterojunctions between them have been applied to resolve the limitations of TiO_2 [5,8]. As an alternative strategy, the developing of new materials that are activated under visible light and induced the separation of charge carriers has therefore turned into an ongoing research worldwide [8,9].

In recent years, bismuth-based photocatalysts such as Bi_2MoO_6, Bi_2O_3 and Bi_2WO_6 have been commonly used under visible light irradiation owing to their low toxicity, abundance and favorable photocatalytic performance [10-13]. Moreover, a special focus has been placed on Bi_2WO_6 as a cost-effective n-type semiconducting photocatalyst with unique physicochemical properties such as appropriate optical gap and chemical stability [14]. Bi_2WO_6 structure belongs to the Aurivillius family, which is constructed from the alternative layers of $(Bi_2O_2)^{2+}$ layer and perovskite-like layer of $(WO_4)^{2-}$ [15]. This unique structure causes the effective separation of photogenerated electrons from holes produced under light irradiation due to the electric field between $(Bi_2O_2)^{2+}$ and $(WO_4)^{2-}$ layers, which decreases the recombination of charge carriers and thus improves photocatalytic performance [16,17]. Xu et al. reported the synthesis of ultra-thin Bi_2WO_6 porous nanosheets which exhibited excellent photocatalytic activities under visible light for the degradation of pollutants in water [18]. Zhang et al. synthesized Bi_2WO_6 nanoplates with laminar morphology and applied for photocatalytic degradation of organic compounds under visible light [19]. Shivani et al. reported that 99.8% of the dye molecules degraded in 160 min under visible light irradiation [20]. Despite numerous studies on the photocatalytic applications of this compound, its photocatalytic efficiency has remained unacceptable. The limitations of this compound include short lifetime of the electrons-holes produced and weak optical absorption [21,22].

Different methods proposed to overcome the application limitations of Bi_2WO_6 include smearing the nanoparticles of noble metals such as silver onto the Bi_2WO_6 surface to cause surface plasmon resonance of the metal nanoparticles and thereby improve the optical absorption and photocatalytic performance of the compound [23]. The photocatalytic performance of the Bi_2WO_6 compound can also be enhanced by creating oxygen vacancies in its structure to trap electrons or holes and reduce the recombination rate of charge carriers [24]. Moreover, Bi_2WO_6 can be easily combined with other semiconductors to create heterostructured photocatalysts, which causes the effective spatial separation of electrons from holes and reduces their recombination likelihood [25-27].

†To whom correspondence should be addressed.
E-mail: tahmasebi@jsu.ac.ir

The reports published to date have introduced combining Bi_2WO_6 with other semiconductors and forming heterostructured as a highly-effective method in improving the photocatalytic performance of Bi_2WO_6.

On the other hand, very high photocatalytic performance in degrading aqueous organic pollutants has been reported for bismuth oxyhalides, including BiOCl, BiOBr and BiOI, as a new group of photocatalysts [27,28]. The present study therefore aimed at examining the effect of adding a bismuth oxyhalide on the photocatalytic performance of Bi_2WO_6. The hybrid samples were synthesized using a simple one-stage hydrothermal method. This technique is environmentally safe because all the reactions take place in a closed ambient, with a low energy requirement for synthesis of nanomaterials [29]. It is well known that this synthesis method has the potential to contribute industrially due to its simple approach [30]. The synthesized samples were characterized using XRD, SEM, DRS and the nitrogen absorption/desorption technique. The performance of the samples was then investigated in terms of the photocatalytic degradation of the aqueous RhB solution under visible light irradiation. The results showed that the highest photocatalytic performance under visible light irradiation was associated with the hybrid Bi_2WO_6/BiOBr photocatalyst compared to that of pure Bi_2WO_6 and combination samples of Bi_2WO_6/BiOCl and Bi_2WO_6/BiOI.

EXPERIMENTAL SECTION

1. Sample Preparation

To synthesize the samples using the hydrothermal method, 1.11 g of sodium tungstate dehydrate ($Na_2WO_4{\cdot}2H_2O$) dissolved in 50 ml of deionized water was stirred in a magnetic stirrer for 60 min. Another beaker containing 2.13 g of bismuth nitrate pentahydrate ($Bi(NO_3)_3{\cdot}5H_2O$), 0.50 g of polyvinylpyrrolidone and 0.60 mL of HX acid (X=Cl, Br and I) dissolved in 50 ml of deionized water was placed on the magnetic stirrer for 30 min. The final solution obtained through the dropwise addition of the first solution to the second was stirred for 10 min, then transferred to a 100-ml autoclave chamber and heated at 180 °C for 12 hours and allowed to naturally cool at room temperature. The precipitates obtained from centrifuging and rinsing were ultimately dried for 4 hours at 80 °C. A pure Bi_2WO_6 sample was also synthesized in the absence of an acid.

2. Characterization

A Philips X'Pert X-ray diffractometer with CuKα radiation (λ= 1.54178 Å) was used at 2θ=10°-70° to identify the phase and crystal structure of the products. The morphology and chemical composition of the samples were determined using a Tescan Vega scanning electron microscope equipped with an energy dispersive spectrometer. DRS was performed using a UV visible spectrometer (Avaspec-2048-TEC model) at a wavelength of 200-800 nm with $BaSO_4$ as the reference. The specific surface area of the samples was also measured using nitrogen absorption/desorption isotherms and the BET method (BESORP mini II). The photoluminescence (PL) emission spectra were measured using a spectrometer with the excitation wavelength of 360 nm.

3. Photocatalytic Activity

The photocatalytic activity of the synthesized samples was investigated under the irradiation of a 55-W Xenon lamp using the RhB aqueous solution as the source of pollution. All the UV rays of the Xenon lamp with a wavelength of below 420 nm were filtered to ensure that the photocatalytic reaction was affected only by visible light. In each experiment, 45 mg of the photocatalyst was added to 45 mL of a 10 mg/L RhB dye solution. This solution underwent visible light irradiation after being placed in the dark for an hour to reach the absorption-desorption equilibrium. The beaker containing the photocatalyst solution was placed in ice-water to cool during irradiation. A magnetic stirrer was also used to disperse the photocatalyst particles in the solution. 2 mL of the dye solution was then removed every 20 min, centrifuged and its UV-vis spectra were measured and the concentration of the residual dye was calculated using the absorption peak of RhB at 554 nm.

RESULTS AND DISCUSSION

1. Materials Characterization

Fig. 1 shows the XRD patterns of the samples synthesized in the absence of an acid and in the presence of HCl, HBr and HI. Given the diffraction peaks of the sample synthesized in the absence of an acid (Fig. 1(a)), all the peaks matched the tetragonal crystal structure of Bi_2WO_6 according to JCPDS No. of 26-1044. Fig. 1(b)-(d) also suggests the dominant peaks of the samples synthesized in the presence of different acids are associated with the tetragonal crystal structure of Bi_2WO_6. For synthesized samples in the presence of HCl, HBr and HI, in addition to the peaks associated with the tetragonal crystal structure of Bi_2WO_6, weaker peaks appear-

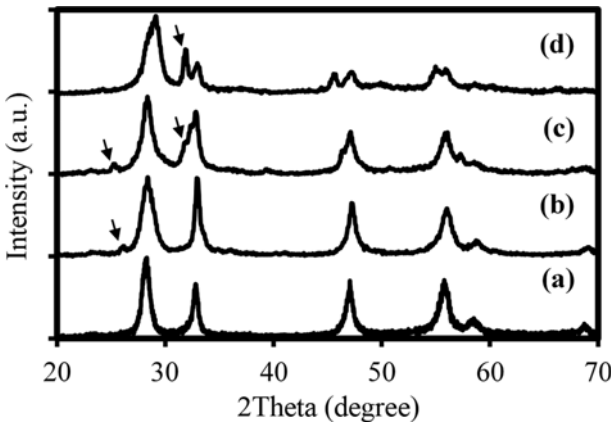

Fig. 1. XRD patterns of the samples synthesized (a) in the absence of an acid, and in the presence of (b) HCl, (c) HBr and (d) HI.

Table 1. The atomic percentage of the constituent elements of (a) Bi_2WO_6, (b) Bi_2WO_6/BiOCl, (c) Bi_2WO_6/BiOBr, and (d) Bi_2WO_6/BiOI

	Bi (%)	W (%)	O (%)	Cl (%)	Br (%)	I (%)
(a)	15.06	11.14	73.80	-	-	-
(b)	14.69	10.14	71.53	3.64	-	-
(c)	14.88	10.32	71.07	-	3.73	-
(d)	16.66	7.77	71.66	-	-	3.91

ing in every spectrum shown as arrows in Fig. 1 can be, respectively, attributed to the crystal structures of BiOCl (JCPDS No 06-0249), BiOBr (JCPDS No 09-0393) and BiOI (JCPDS No 73-2062) in each sample.

Table 1 presents the atomic percentage of the constituent elements of individual samples obtained from performing energy dispersive spectroscopy to identify the chemical composition of the samples. These results showed only bismuth, tungsten and oxygen in the composition of the sample synthesized in the absence of an acid, which suggests the purity of this sample and the formation of Bi_2WO_6. In addition to bismuth, tungsten and oxygen, small percentages of chlorine, bromine and iodine were, respectively, observed in the compositions of the samples synthesized in the presence of HCl, HBr and HI. These results confirmed the XRD findings and showed the possibility of the presence of BiOCl, BiOBr and BiOI and the formation of Bi_2WO_6/BiOCl, Bi_2WO_6/BiOBr and Bi_2WO_6/BiOI in the presence of these acids, respectively.

SEM was performed to determine the morphology of the samples. Fig. 2 shows the SEM images of the samples obtained at two magnifications in the absence of an acid and in the presence of

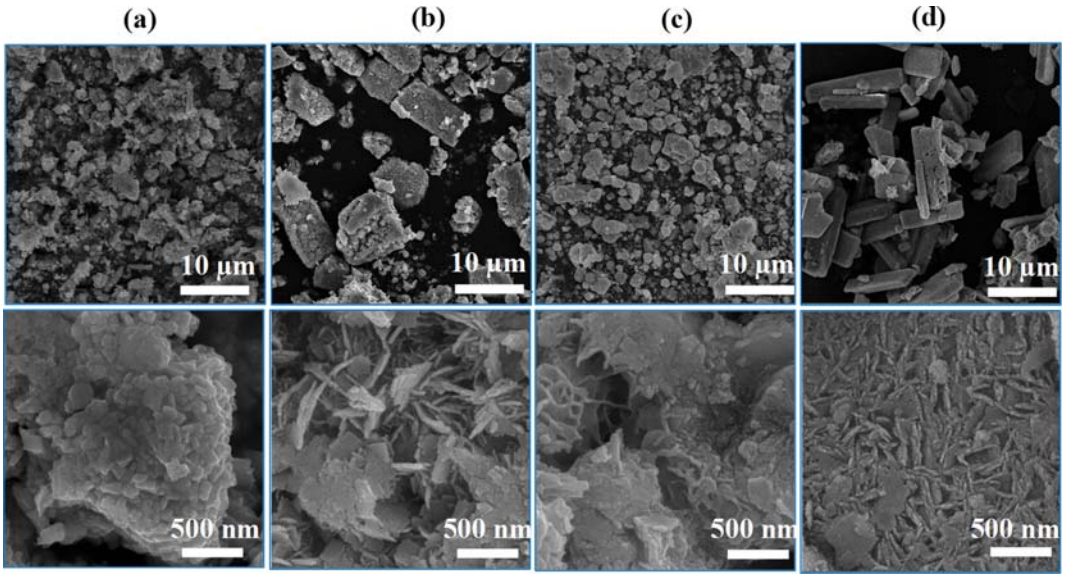

Fig. 2. SEM images of the samples obtained at two magnifications (a) Bi_2WO_6, (b) Bi_2WO_6/BiOCl, (c) Bi_2WO_6/BiOBr, and (d) Bi_2WO_6/BiOI.

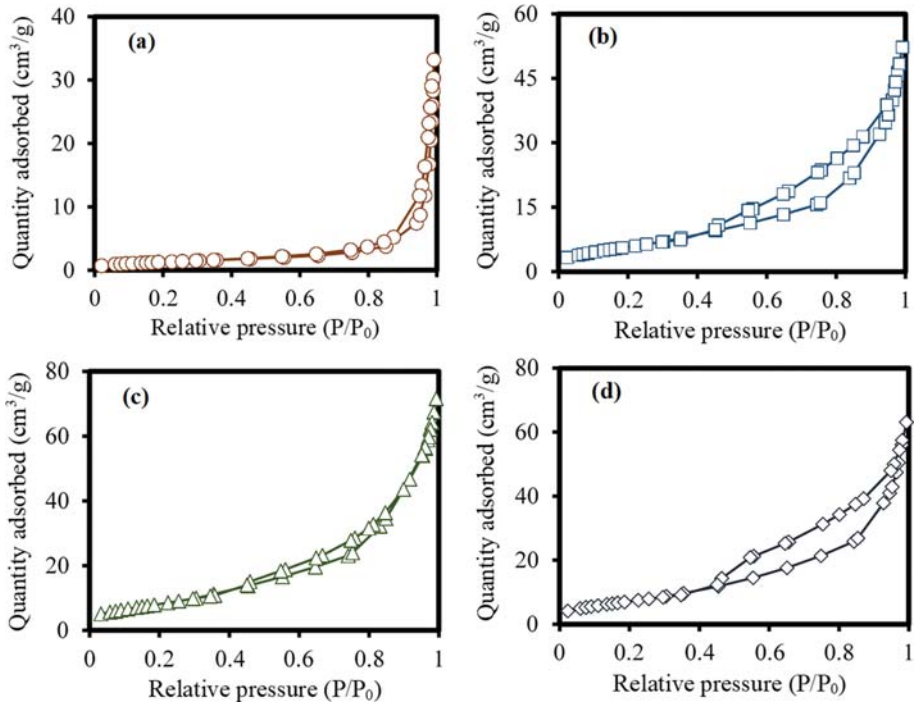

Fig. 3. The N_2 adsorption-desorption isotherms of (a) Bi_2WO_6, (b) Bi_2WO_6/BiOCl, (c) Bi_2WO_6/BiOBr, and (d) Bi_2WO_6/BiOI.

HCl, HBr and HI acids. According to Fig. 2(a), the sample synthesized in the absence of an acid comprised particles with below 100-nm dimensions. The samples synthesized in the presence of hydrochloric acid (Fig. 2(b)) and hydroiodic acid (Fig. 2(d)) morphologically comprised microcubes made of several nanosheets seemingly associated with BiOCl and BiOI given the reported tendency of oxyhalides to form nanostructured sheets [31,32]. The SEM of the sample synthesized in the presence of hydrobromic acid (Fig. 2(c)) showed particles with approximately 1 μm dimensions in its structure. Increasing magnification showed that each of the microparticles was made up of a combination of nanoparticles and nanosheets, respectively, associated with Bi_2WO_6 and BiOBr.

The specific surface area of the samples was measured using the nitrogen absorption-desorption technique at 77 °K. Fig. 3 illustrates the N_2 adsorption-desorption isotherms of individual samples, showing the type-3 isotherm of pure Bi_2WO_6 that suggests weak interaction between the N_2 molecules and the absorbent. The isotherms of all the three hybrid samples shown in Fig. 3(b)-(d) match type 4 with a hysteresis loop at a relative pressure of 0.5-1, suggesting mesoporous structure. Table 2 presents the specific surface area and pore size and diameter, associating the largest effective surface area with Bi_2WO_6/BiOBr (29.86 m^2g^{-1}), resulting in the maximum potential number of active sites on its surface. It is expected that the adsorption of RhB molecules on the photocatalyst surface is therefore maximized and the photocatalytic performance of this sample improves [32,33]. Table 2 also shows the higher pore volume of Bi_2WO_6/BiOBr compared to that of the other samples. The larger the pore size, the greater the penetration of light and pollutant's molecules into a photocatalyst and the higher both the likelihood of charge carrier formation and the photocatalytic efficiency

Table 2. Specific surface area and pore size and diameter of (a) Bi_2WO_6, (b) Bi_2WO_6/BiOCl, (c) Bi_2WO_6/BiOBr, and (d) Bi_2WO_6/BiOI

	S_{BET} (m^2g^{-1})	Pore volume (cm^3g^{-1})	Pore diameter (nm)
(a)	4.773	0.048	7.97
(b)	21.178	0.080	1.93
(c)	29.866	0.107	2.45
(d)	26.448	0.094	1.29

[33,34].

Diffuse reflectance spectroscopy (DRS) can help determine optical properties such as optical absorption and the energy gap with known key roles in the photocatalytic activity of semiconductors. Fig. 4(A) shows the absorption spectra of the samples. The energy gap in a crystal semiconductor can be calculated using $\alpha h\nu = (h\nu - E_g)^n$ [35-37], where α represents the absorption coefficient, ν frequency, h the Planck constant and E_g the energy gap, while the conduction-dependent n equals 2 in semiconductors with an indirect gap and 0.5 with a direct gap. The energy gap can be calculated through the extrapolation of a tangent line to the linear portion of $(\alpha h\nu)^{1/n}$. Fig. 4(B) shows the energy gap of pure Bi_2WO_6 was 2.50 eV, that of Bi_2WO_6/BiOCl 2.52 eV, Bi_2WO_6/BiOBr 2.80 eV and Bi_2WO_6/BiOI 1.88 eV. All the energy gaps lying in the visible spectrum suggested the potential photocatalytic activity of all the samples under visible light irradiation.

2. Photocatalytic Performance

The photocatalytic performance of the samples was then examined in degrading the aqueous RhB solution as the pollution model. The concentration of RhB in water was determined by recording variation in the intensity of its absorption peak at 554 nm. Fig. 5(A) shows the absorption spectrum of the aqueous RhB solution in the presence of Bi_2WO_6/BiOBr under visible light irradiation, suggesting a shift in the absorption peak of the dye toward shorter wavelengths with a decrease in the intensity. Moreover, color changes were observed in the dye from pink to orange, then yellow and eventually colorlessness during the irradiation. Research attributes this shift and change in color to the step-by-step degradation of RhB molecules in the solution and deethylation in the dye degradation [31,38].

Fig. 5(B) shows changes in the dye concentration by irradiation duration, suggesting an approximate degradation of 98% in the dye by Bi_2WO_6/BiOBr, 40% degradation by pure Bi_2WO_6, 65% degradation by Bi_2WO_6/BiOCl and 26% by Bi_2WO_6/BiOI, all under 80 min irradiation. Fig. 5(C) shows the diagram of $Ln(C/C_0)$ versus time and a line fitted on data, which shows a linear trend. The degradation kinetics of RhB in all the samples therefore appears to follow the pseudo-first-order equation of $Ln(C/C_0)=kt$, in which C_0 and C, respectively, represent the initial RhB concentration and its concentration at time t and k the kinetic constant, i.e., the dye

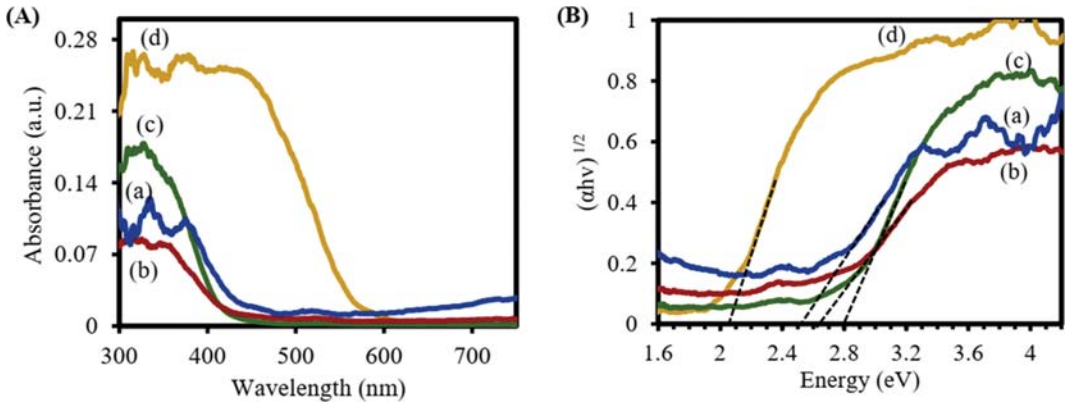

Fig. 4. (A) UV-vis absorption spectra and (B) the energy gap of (a) Bi_2WO_6, (b) Bi_2WO_6/BiOCl, (c) Bi_2WO_6/BiOBr, and (d) Bi_2WO_6/BiOI.

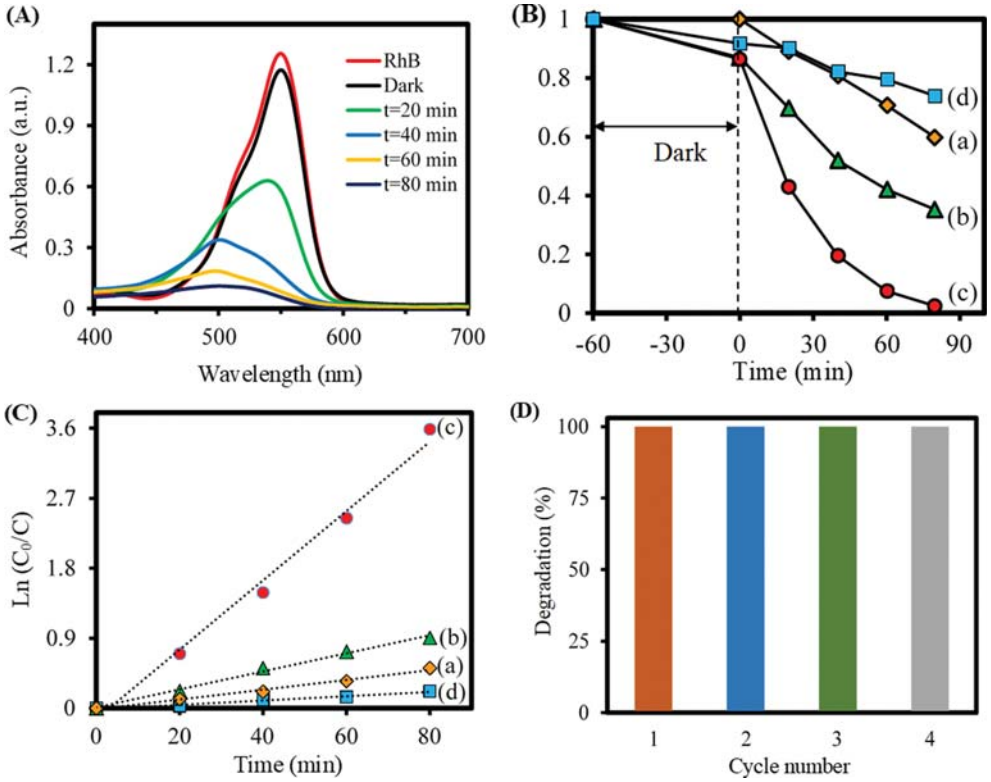

Fig. 5. (A) Absorption spectrum of the aqueous RhB solution in the presence of Bi_2WO_6/BiOBr, (B) photocatalytic performance, (C) the Ln (C_0/C) versus time curves, and (D) the photocatalytic performance of Bi_2WO_6/BiOBr sample in four successive cycles. (a) Bi_2WO_6, (b) Bi_2WO_6/BiOCl, (c) Bi_2WO_6/BiOBr, and (d) Bi_2WO_6/BiOI.

degradation rate [39,40]. According to the results, the photocatalytic performance of Bi_2WO_6/BiOBr was higher than that of the other samples given its highest degradation rate: k~0.042 min^{-1}. Given stability and repeatability as important characteristics of a photocatalyst in practical applications, the repeatability of Bi_2WO_6/BiOBr was examined. Fig. 5(D) shows the results of investigating the photocatalytic performance of this sample in four successive cycles, suggesting its relatively constant efficiency in RhB degradation under the same conditions and its stability during repeated photocatalytic processes.

3. Photocatalytic Mechanism

The optical gap, effective surface area and ability to separate electrons from holes play a key role in the photocatalytic activity of semiconductors. According to the DRS, the optical absorption ability of Bi_2WO_6/BiOI was higher and its energy gap lower than those of the other samples, whereas its photocatalytic efficiency was the lowest. According to the experimental results obtained, irrespective of the energy gap, the relatively higher photocatalytic performance of Bi_2WO_6/BiOBr can be explained by its largest effective surface area and strong interactions between Bi_2WO_6 and BiOBr, which reduces recombination and effectively separates the charge carriers produced at the interface between adjacent semiconductors [41]. The performance of samples to separate the photogenerated charge carriers was investigated by PL spectra. Fig. 6 shows the PL spectrum of pure Bi_2WO_6, Bi_2WO_6/BiOCl, Bi_2WO_6/BiOBr and Bi_2WO_6/BiOI samples. It is observed the intensity of emission spectrum of Bi_2WO_6/BiOBr and Bi_2WO_6/BiOI is lower than other

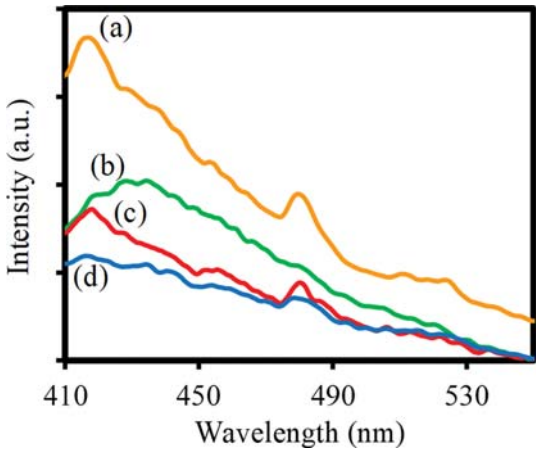

Fig. 6. PL spectrum of (a) Bi_2WO_6, (b) Bi_2WO_6/BiOCl, (c) Bi_2WO_6/BiOBr, and (d) Bi_2WO_6/BiOI.

samples, indicating the lowest recombination of photogenerated charge carriers. However, due to the poor photocatalytic activity of Bi_2WO_6/BiOI, its low PL spectrum may be attributed to the low electron-hole formation.

In photocatalytic processes, organic pollutants are degraded on the surface of a semiconductor by the active species produced [42]. An active species trapping test was thus conducted to identify active species participating in the photocatalytic reactions using disodium ethylene diamine tetraacetic acid (EDTA-2Na), tret-butyl

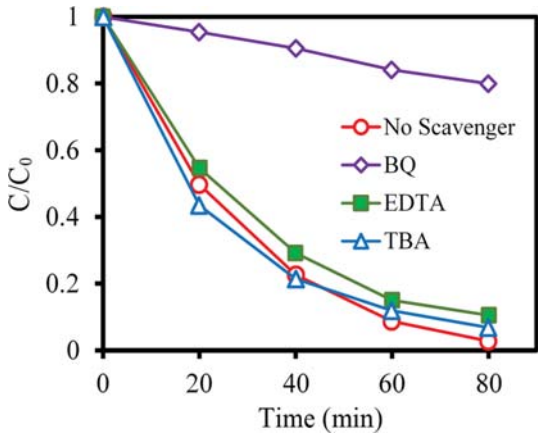

Fig. 7. The photocatalytic performance of Bi_2WO_6/BiOBr sample in the presence of different scavengers.

alcohol (TBA) and benzoquinone (BQ) to, respectively, trap holes, hydroxyl radicals ($^{\bullet}OH$) and superoxide radicals ($^{\bullet}O_2^-$) [43,44]. The effects of these factors were measured in a similar manner as in the photocatalytic performance test. The only difference lay in adjusting the concentration of each of the trapping substances in the dye solution at 1 mM. The results obtained from this analysis and Fig. 7 show the significant effect of BQ and negligible effects EDTA-2Na and TBA on reducing the photocatalytic degradation of RhB dye molecules. The present findings suggest despite the role of holes and hydroxyl radicals in photocatalytic reactions, superoxide radicals play the most critical role in the degradation of RhB molecules.

CONCLUSION

The present study employed the simple single-stage hydrothermal method to synthesize the pure photocatalyst Bi_2WO_6 and the hybrid photocatalysts Bi_2WO_6/BiOX (X=Cl, Br, I). The photocatalytic performance of Bi_2WO_6/BiOBr in degrading RhB molecules under visible light irradiation was found to be the highest compared to that of the other samples. In fact, about 97% of RhB molecules were degraded within 80 min in the presence of this photocatalyst, whereas this figure was 40%, 60% and 20% for pure Bi_2WO_6 and Bi_2WO_6/BiOCl and Bi_2WO_6/BiOI, respectively. The better performance of this sample was attributed to its larger specific surface and strong interactions between Bi_2WO_6 and BiOBr. The test performed to determine active species in the photocatalytic reactions of Bi_2WO_6/BiOBr also found superoxide radicals to play the main role in the degradation of RhB molecules. In addition, the stability of Bi_2WO_6/BiOBr as a hybrid photocatalyst was acceptable and its photocatalytic efficiency high during four successive cycles. This study demonstrates the capability of Bi_2WO_6/BiOBr composite photocatalyst for practical application in degrading environmental pollutants.

REFERENCES

1. Z. Jiang, X. Liang, Y. Liu, T. Jing, Z. Wang, X. Zhang, X. Qin, Y. Dai and B. Huang, *Appl. Catal. B: Environ.*, **211**, 252 (2017).
2. J. Tian, Y. Sang, G. Yu, H. Jiang, X. Mu and H. Liu, *Adv. Mater.*, **25**, 5075 (2013).
3. Y. Cho, H. J. Lee and S. Sung, *Korean J. Chem. Eng.*, **37**, 1071 (2020).
4. R. Qian, H. Zong, J. Schneider, G. Zhou, T. Zhao, Y. Li, J. Yang, D. W. Bahnemann and J. H. Pan, *Catal. Today*, **335**, 78 (2019).
5. G. Žerjav, M. S. Arshad, P. Djinović, I. Junkar, J. Kovač, J. Zavašnik and A. Pintar, *Nanoscale*, **9**, 4578 (2017).
6. H. Liu, W. R. Cao, Y. Su, Z. Chen and Y. Wang, *J. Colloid Interface Sci.*, **398**, 161 (2013).
7. I. Tsuji, H. Kato and A. Kudo, *Chem. Mater.*, **18**, 1969 (2006).
8. S. A. Ansari, M. M. Khan, M. O. Ansari and M. H. Cho, *New J. Chem.*, **40**, 3000 (2016)
9. T. Saison, P. Gras, N. Chemin, C. Chanéac, D. Durupthy, V. Brezova, C. Colbeau-Justin and J. P. Jolivet, *J. Phys. Chem. C*, **117**, 22656 (2013).
10. Y. Jia, Y. Lin, Y. Ma and W. Shi, *Mater. Lett.*, **234**, 83 (2019).
11. C. Wang, C. Shao, L. Wang, L. Zhang, X. Li and Y. Liu, *J. Colloid Interface Sci.*, **333**, 242 (2009).
12. M. Ge, Y. Li, L. Liu, Z. Zhou and W. Chen, *J. Phys. Chem. C*, **115**, 5220 (2011).
13. A. M. Yang, Y. Han, S. S. Li, H. W. Xing, Y. H. Pan and W. X. Liu, *J. Alloys Compd.*, **695**, 915 (2017).
14. A. Kaur and S. K. Kansal, *Chem. Eng. J.*, **302**, 194 (2016).
15. Z. P. Nie, D. K. Ma, G. Y. Fang, W. Chen and S. M. Huang, *J. Mater. Chem.,* A, **4**, 2438 (2016).
16. N. Zhang, R. Ciriminna, M. Pagliaro and Y. J. Xu, *Chem. Soc. Rev.*, **43**, 5276 (2014).
17. F. Xu, C. Xu, H. Chen, D. Wu, Z. Gao, X. Ma, Q. Zhang and K. Jiang, *J. Alloys Compd*, **780**, 634 (2019).
18. F. Xu, H. Chen, C. Xu, D. Wu, Z. Gao, Q. Zhang and K. Jiang, *J. Colloid Interface Sci.*, **525**, 97 (2018).
19. C. Zhang and Y. Zhu, *Chem. Mater.*, **17**, 3537 (2005).
20. V. Shivani, S. Harish, J. Archana, M. Navaneethan, S. Ponnusamy and Y. Hayakawa, *Appl. Surf. Sci.*, **488**, 696 (2019).
21. S. P. Hu, C. Y. Xu and L. Zhen, *Mater. Lett.*, **95**, 117 (2013).
22. Z. Li, L. Zhu, W. Wu, S. Wang and L. Qiang, *Appl. Catal. B: Environ.*, **192**, 277 (2016).
23. Y. Guo, J. Wei, T. Yang, Z. Lv and Z. Xu, *Optik*, **180**, 285 (2019).
24. Z. Zhang, W. Wang, E. Gao, M. Shang and J. Xu, *J. Hazard. Mater.*, **196**, 255 (2011).
25. H. Zhou, Z. Wen, J. Liu, J. Ke, X. Duan and S. Wang, *Appl. Catal. B: Environ.*, **242**, 76 (2019).
26. S. Chaiwichian, B. Inceesungvorn, K. Wetchakun, S. Phanichphant, W. Kangwansupamonkon and N. Wetchakun, *Mater. Res. Bull.*, **54**, 28 (2014).
27. F. Wang, Y. Gu, Z. Yang, Y. Xie, J. Zhang, X. Shang, H. Zhao, Z. Zhang and X. Wang, *Appl. Catal. A: Gen.*, **567**, 65 (2018).
28. Y. Yang, C. Zhang, C. Lai, G. Zeng, D. Huang, M. Cheng and W. Xiong, *Adv. Colloid Interface Sci.*, **254**, 76 (2018).
29. D. Durgalakshmi, R. A. Rakkesh and J. Mohanraj, *Graphene-metal-organic framework-modified electrochemical sensors*, Graphene-Based Electrochemical Sensors for Biomolecules, Elsevier, New York (2019).
30. A. Kumar and D. Nanda, *Methods and fabrication techniques of superhydrophobic surfaces*, Superhydrophobic Polymer Coatings, Elsevier, New York (2019).

31. L. Chen, R. Huang, M. Xiong, Q. Yuan, J. He, J. Jia, M. Yao, S. Luo, C. Au and S. Yin, *Inorg. Chem.*, **52**, 11118 (2013).
32. J. Xiong, G. Cheng, G. Li, F. Qin and R. Chen, *RSC Adv.*, **1**, 1542 (2011).
33. M. Thommes, K. Kaneko, A. V. Neimark, J. P. Olivier, F. Rodriguez-Reinoso, J. Rouquerol and K. S. Sing, *Pure Appl. Chem.*, **87**, 1051 (2015).
34. Z. Jiang, X. Liang, Y. Liu, T. Jing, Z. Wang, X. Zhang, X. Qin, Y. Daib and B Huang, *Appl. Catal. B: Environ.*, **211**, 252 (2017).
35. L. Huang, W. Fang, Y. Yang, J. Wu, H. Yu, X. Dong, T. Wang, Z. Liu and B. Zhao, *Mater. Res. Bull.*, **108**, 38 (2018).
36. L. Zhang, C. G. Niu, G. X. Xie, X. J. Wen, X. G. Zhang and G. M. Zeng, *ACS Sust. Chem. Eng.*, **5**, 4619 (2017).
37. A. L. Lu, M. Y. Zhou, L. Yin, G. W. Zhou, T. Jiang, X. K. Wan and H. X. Shi, *J. Mol. Catal. A: Chem.*, **423**, 379 (2016).
38. X. Meng and Z. Zhang, *J. Photochem. Photobiol. A: Chem.*, **310**, 33 (2015).
39. P. Intaphong, A. Phuruangrat, S. Thongtem and T. Thongtem, *Mater. Lett.*, **213**, 88 (2018).
40. Q. Sun, X. Jia, X. Wang, H. Yu and J. Yu, *Dalton Trans.*, **44**, 14532 (2015).
41. N. Tahmasebi, Z. Maleki and P. Farahnak, *Mater. Sci. Semicond. Process.*, **89**, 32 (2019).
42. X. Jia, J. Cao, H. Lin, M. Zhang, X. Guo and S. Chen, *Appl. Catal. B: Environ.*, **204**, 505 (2017).
43. Y. Ao, K. Wang, P. Wang, C. Wang and J. Hou, *RSC Adv.*, **6**, 48599 (2016).
44. K. Wang, C. Shao, X. Li, X. Zhang, N. Lu, F. Miao and Y. Liu, *Catal. Commun.*, **67**, 6 (2015).